

Molecular Insights into NO-Promoted Sulfate Formation on Model TiO₂ Nanoparticles with Different Exposed Facets

Weiwei Yang,[†] Min Chen,[‡] Wen Xiao,[§] Yanbing Guo,^{*,†} Jun Ding,[§] Lizhi Zhang,[†] and Hong He[‡]

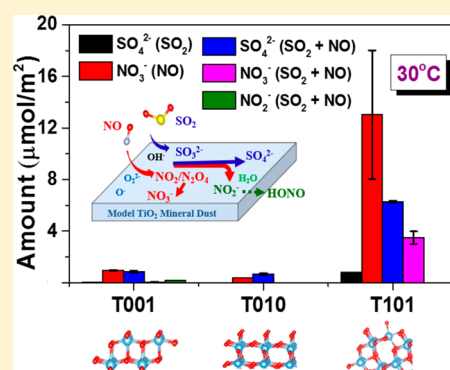
[†]Key Laboratory of Pesticide and Chemical Biology of Ministry of Education, Institute of Environmental and Applied Chemistry, College of Chemistry, Central China Normal University, Wuhan 430079, China

[‡]State Key Joint Laboratory of Environment Simulation and Pollution Control, Research Center for Eco-Environmental Sciences, Chinese Academy of Sciences, Beijing 100085, China

[§]Department of Materials Science and Engineering, National University of Singapore, Singapore 119260, Singapore

Supporting Information

ABSTRACT: In this study, molecular insights into NO-promoted SO₂ oxidation on model TiO₂ with well-defined (001), (010), and (101) facets are investigated in the laboratory. The adsorbed SO₂ is significantly promoted to transform into sulfate by the coexisting NO on the three facets. The appearance of active oxygen species indicates an active oxygen species-initiated NO oxidation. The resulting NO₂ acts as an oxidant to convert adsorbed sulfite on hydroxyls to sulfate species. The (101) facet presents the best performance in the NO-promoted sulfate formation possibly owing to its desirable structure to accommodate SO₃²⁻, NO₂, and molecular water. The uptake coefficient (γ_t) of SO₂ increases by the coexistence of NO on the (001) facet at 0% RH and is relative humidity (RH) dependent, which first decreases from 0% RH to 32% RH but then increases in the range of 32%–80% RH. The probable explanation is the combined contribution of the blocking effect of water and the hydration of SO₂. The finding in this study provides insight into the possibility of its occurrence on common mineral dusts and requires further investigation.



INTRODUCTION

Sulfate aerosol evolution can cause severe environmental issues, including photochemical smog, acid rain, and haze formation.^{1–3} Mineral dust represents a dominant mass fraction of atmospheric particulate matter with increasing emissions from erosion, mining, and industrial activities of 1000–3000 Tg per year.⁴ In an ambient atmosphere, the heterogeneous reaction of sulfur dioxide (SO₂) on mineral dust has been shown to be of great importance in sulfate formation. Lab and field studies confirm that the incorporation of transition metal-involved, heterogeneous oxidation of SO₂ into models could effectively close the gap between the observed and simulated sulfate results.⁵

Industrially manufactured TiO₂ nanomaterials have been the main concern because of their wide range of applications, such as pigments, sensors, building blocks, and catalysts.^{6–8} It is suggested that these nanomaterials have a great chance of entering in the environments during production and application, giving rise to high-activity suspended aerosols.⁸ Thus, molecular-level insights into the surface adsorption and transformation of SO₂ on well-engineered TiO₂ particles have been a popular focus of lab investigations.^{9,10} The photochemical reaction of SO₂ on TiO₂ has been paid the largest amount of attention due to the unique photochemical property of TiO₂.^{11–13} The predominant sulfite species that form during exposure to SO₂ on TiO₂ particles in the dark can be converted to sulfate species upon irradiation at ambient temperatures,⁹

while those releasing engineered TiO₂ nanomaterials vary in morphology, hence attracting researchers in the modeling of the TiO₂ surfaces that are involved in heterogeneous chemistry.^{8,14,15} For example, on single-crystal TiO₂ (110), SO₂ interacts weakly with the nearly perfect surface, but it reacts vigorously with defect surfaces to form sulfate species under ultrahigh vacuum conditions.¹⁵ To our knowledge, however, the heterogeneous chemistry of SO₂ on TiO₂ nanomaterials in the vicinity of industrial areas has seldom been paid attention.

In the industrial areas, such as coal-fired power plants, catalysis technology enables the effective control of SO₂ and NO_x emissions but leads to an unanticipated increase in the emission of sulfate aerosols around the source vents.^{16–19} The pathways for SO₂ reactions under this circumstance are hardly evaluated in the context of the coexisting multiple effluents, such as SO₂, water vapor, NO_x, and fly ash.^{16,19} Most studies attribute the increased emission of sulfate to the enhanced gas-phase conversion of SO₂ initiated by OH radicals in plumes. Other hypotheses are built on the in-stack formation of sulfate, such as the interaction of SO₂ with adsorbents or coexisting gases. The concentration of NO emitted from stationary

Received: May 20, 2018

Revised: October 22, 2018

Accepted: November 5, 2018

Published: November 5, 2018

sources is high, largely at the ppmv level.^{20,21} Previous studies found that NO can promote the oxidation of SO₂ on CaO and Al₂O₃ at 150 °C in the flue gas removal process,^{22,23} while there exists great controversy as to the intermediates, such as nitro or SO₃-NOx compounds. Recent ambient atmospheric chemistry has found a significant promotion role of NO₂ in the conversion of SO₂ to sulfate on mineral dusts, during which the released NO product may involve the regeneration of NO₂.^{24,25} Evidently, verification of the role of NO in the sulfate formation and elucidation of the reaction mechanism appear to be of great importance. Especially under atmospherically relevant conditions, no attention has been paid to the influence of NO on the sulfate formation. Moreover, the effect of different exposed facets on sulfate formation, which is critical for the optimum design of industrial TiO₂-based catalysts to balance sulfate formation and toxic gas purification, has also not been elucidated.

In this study, we chose the commonly engineered anatase TiO₂ facets, (001), (101), and (010), as model nanoparticles, to determine the reaction pathway of SO₂ with the coexistence of NO under simulated conditions. A possible NO-promoted mechanism for the formation of sulfate is proposed by combining diffuse reflectance infrared Fourier transform spectroscopy (DRIFTS), flow tube reactor, and ion chromatography (IC). This work will help deepen our understanding of the undesired source of sulfates in industrial areas containing NO as well as well-engineered nanomaterials. It also sheds light on the rational design of specific facet exposed TiO₂ nanocatalysts in industrial applications containing both NO and SO₂.

MATERIALS AND METHODS

Materials. The preparation of anatase TiO₂ nanoparticles with dominant (001), (010), and (101) facets (denoted as T001, T010, and T101 in the following text) and relevant physical characterization of the as-synthesized samples are described in the [Supporting Information](#). T001 was used as a coated sample in a quartz tube (20 cm length, 1.0 cm i.d.) positioned inside the flow tube reactor. 0.4 g of T001 powder was dissolved in 20.0 mL of ethyl alcohol. The suspension was dispersed uniformly in the quartz tube and dried overnight in an oven at 150 °C, resulting in a homogeneous film covering the entire inner surface of the quartz tube.

DRIFTS Reactions. DRIFTS spectra were collected (4000–600 cm⁻¹) with a resolution of 4 cm⁻¹ using a Fourier transform infrared spectrometer (Nicolet is50, Thermo Fisher Scientific Co., USA) equipped with a Harrick DRIFTS cell and a MCT/A detector. The sample was first pretreated at 300 °C for 30 min and cooled down to the target temperature step by step to obtain the background. Subsequently, the sample was exposed to a gas mixture of 500 ppmv NO, 5 vol % O₂, and N₂ (or 50 ppmv SO₂ + 5 vol % O₂ + N₂ or 500 ppmv NO + 5 vol % O₂ + 50 ppmv SO₂ + N₂) at 30 °C for 40 min in a total flow of 300 mL min⁻¹. The following temperature-programmed reaction was recorded at an elevated temperature from 30 to 400 °C after the reaction temperature stabilizes at each target temperature. The preadsorption experiments were conducted by exposing the pretreated sample to NO + O₂ (or SO₂) for a specific time interval at 30 °C (or 180 °C) and were followed by purging with N₂ until the spectra no longer changed; another gas was then switched onto the sample surface accordingly.

Besides, the NO and SO₂ adsorption modes on the three facets were further theoretically investigated by adopting the DFT calculations. The selection of structural models and details of the electronic structure calculations are given in the [Supporting Information](#).

Flow Tube Reactor. The heterogeneous uptake of SO₂ in the absence and presence of NO was carried out in a horizontal cylindrical coated-wall flow tube reactor (34 cm length, 1.6 cm i.d.), as described in detail in previous studies and similar to that used by Ndour et al.^{26–28} The experiments were performed at 25 °C by circulating water through the outer jacket of the flow tube reactor. Zero air was introduced in the flow tube as the carrier gas, and the total flow rate was 1.4 L min⁻¹ to ensure a laminar regime. The RH was adjusted by varying the ratio of dry zero air to wet zero air and online monitored using a Vaisala HMP110 probe. SO₂ and/or NO were brought into the flow tube reactor via a movable injector (0.3 cm o.d.). The concentrations of SO₂ and NO were online measured by using an SO₂ chemiluminescence analyzer (THERMO 43i) and an NOx chemiluminescence analyzer (THERMO 42i), with the inlet concentration at (210 ± 5) ppb and (240 ± 2) ppb, respectively. Since the formed HONO can also be detected as NO₂ by the analyzer, a Na₂CO₃ denuder tube (10 cm length, 0.8 cm i.d.) was put between the exit of the flow tube reactor and the analyzer to trap HONO.^{26,29}

There is a great probability for SO₂ to diffuse into the internal surface of the powdered sample. Thus, the BET surface area was used to calculate the true uptake coefficient (γ_t), which was considered as the lower limit of the uptake coefficient.³⁰ The calculation method was the same as those previously reported, and a detailed description about this is available in the [Supporting Information](#).^{26,27,29}

Surface and Gas Product Analysis. For the surface-adsorbed products, the reacted samples in the DRIFTS cell under different conditions were collected and protected with 1% formaldehyde to prevent the oxidation of sulfite, which were then analyzed by IC (ICS-900, Dionex Corporation) equipped with an AS14A anionic analytical column, an AG14A anionic guard column, and an additional ASRS (300 4 mm) electrolytic suppressor.

To detect the gas products in the heating process, the obtained T001 sample that has been saturated with 500 ppmv NO + 5 vol % O₂ or 500 ppmv NO + 50 ppmv SO₂ + 5 vol % O₂ in the DRIFTS cell at 30 °C was heated from 30 to 450 °C with a ramp rate of 10 °C min⁻¹. The outlet gas flow was diluted to 1.9 L min⁻¹ by zero air and online detected using an NOx chemiluminescence analyzer (THERMO 42i) and an HONO analyzer (Zhichen Technology, China).

RESULTS AND DISCUSSION

SO₂/NO + O₂ Reaction. To investigate the heterogeneous reactions of SO₂ and NO with different TiO₂ facets, *in situ* DRIFTS experiments coupled with theoretical calculation are employed. The detailed spectra of TiO₂ with exposure to SO₂ or NO at the target temperature are shown in [Figure 1](#), [Figure 2](#), and [Figure S3](#). The optimized adsorption configurations of SO₂, SO₃²⁻, SO₄²⁻, NO, NO₂, and NO₃⁻ and their adsorption energies on the three types of faceted samples are provided in [Figure S2](#). As shown in [Figure 1a](#), at 30 °C, the reaction of SO₂ on the surface is weak, leading to the formation of a small amount of sulfite species at the band of 1046 cm⁻¹.³¹ As the temperature increases, the band weakens and almost vanishes

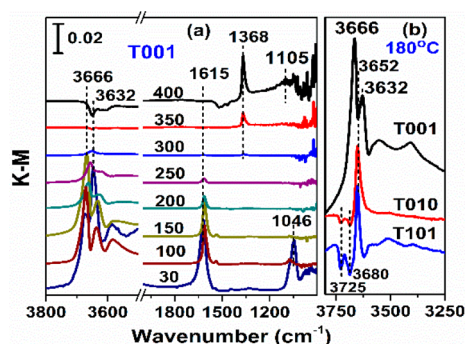


Figure 1. Steady DRIFTS spectra of $\text{SO}_2 + \text{O}_2$ adsorption on (a) T001 as a function of temperature and on (b) three faceted- TiO_2 at 180°C . Reaction conditions: 50 ppmv SO_2 and 5 vol % O_2 balanced with N_2 in a total flow of 300 mL/min under dry conditions.

beyond 100°C . Once the temperature rises above 300°C , new bands, which are ascribed to sulfate, appear at 1368 and 1105 cm^{-1} .^{32,33} A similar adsorption behavior of SO_2 also occurs on the other two samples; relevant spectra are not provided here. The DFT results from Figure S2a show that the SO_2 and SO_3^{2-} are positioned above all the facets, confirming the weak adsorption of SO_2 and its sulfite form. The DFT calculations basically support the DRIFTS results.

The high-frequency region of $3750\text{--}3600\text{ cm}^{-1}$ is dominated by several narrow and partly resolved bands of OH groups.^{34–36} It has been proposed that the band near 1615 cm^{-1} can be assigned to the dissociated adsorption of H_2O , which may originate from the water molecules present in the gas flow.^{37,38} There was the same trend of OH with adsorbed water as the temperature increased. This indicates that the produced OH can be associated with the dissociation of water molecules in oxygen vacancies existing on the highly low-coordinated TiO_2 . Especially for the (001) facet, the richness of oxygen defects derived from its highly low-coordinated structures is most favorable for the production of OH (Figure 1b).^{38,39} It is commonly recognized that the OH groups are principal sites for the adsorption of SO_2 , as presented by the consumption of OH along with the simultaneous generation of sulfate at 400°C in this study.^{31,38,40} The OH ($3725, 3680\text{ cm}^{-1}$) consumption and OH (3652 cm^{-1}) generation arise together on T010 and T101 at 180°C (Figure 1b). The consumed OH can be offset by the generated OH, or otherwise their bands overlapped, thus no observation of the negative bands of OH on T001 at low temperatures.

The DRIFTS spectra for the individual reaction of NO is recorded as a function of temperature from 30 to 400°C , as shown in Figure 2. The detailed assignments of the vibrational bands of the surface species that formed on the three samples are summarized in Table 1. At 30°C , all the facets show high

Table 1. Assignment of Vibrational Bands of Surface Products Formed in the Duration of NO with TiO_2

wavenumber (cm^{-1})	assignment
1980, 1914, 1705 cm^{-1}	NO-Ti^{IV} /gaseous NO ^{35,44,45}
1765–1750 cm^{-1}	N_2O_4 ^{24,47,48}
1625–1616 cm^{-1}	bridging nitrate ^{24,42–44,47,49}
1585–1581, 1246–1233 cm^{-1}	bidentate nitrate ^{24,46,47}
1547–1500, 1292–1287 cm^{-1}	monodentate nitrate ^{41–45}
1185 cm^{-1}	nitrite ^{35,50}
887–808 cm^{-1}	peroxo species ³⁵

reactivity toward NO, which causes three types of nitrate bands developed in the region of $1700\text{--}1000\text{ cm}^{-1}$. On T001, the bridging nitrate is predominant on the surface, with the band appearing near 1625 cm^{-1} ,^{41,42} while the buildup of monodentate nitrate species is more evident on T010 and T101, as demonstrated by the bands at $1547\text{--}1500\text{ cm}^{-1}$ and $1292\text{--}1287\text{ cm}^{-1}$.^{41–45} The rest of the bands at $1585\text{--}1581\text{ cm}^{-1}$ and $1246\text{--}1233\text{ cm}^{-1}$ is attributed to bidentate nitrate, which varies little on the three facets.^{35,45,46} Besides, nitrite species at the band of 1185 cm^{-1} also appear in a time-dependent reaction but vanish quickly due to transformation into stable nitrate species (shown in Figure S3).³⁵

Note that the band of bridging nitrate can be partially overlapped with that of H_2O , which is observed at 1615 cm^{-1} in Figure 1a. However, there is still some controversy as to its assignment. For instance, Huang et al. attributed it to gaseous NO_2 .⁴³ Evidence from the DFT calculations (Figure S2b) in this study implies that the bridging nitrate species seem more thermodynamically stable than gaseous NO_2 since it has lower optimized adsorption energy. Hence, the gaseous NO_2 favors transformation into stable bridging nitrates, while partial NO_2 may also remain, mostly as N_2O_4 dimer at low temperatures, as observed with the feature band at ca. 1765 cm^{-1} .⁴⁷

For the other three discernible bands in the region of $2000\text{--}1700\text{ cm}^{-1}$, i.e. ca. $1980, 1914,$ and 1705 cm^{-1} , they are attributed to the weakly adsorbed NO onto the exposed Ti atom (or oxygen vacancies).^{35,45} These results are supported by the DFT calculation that NO adsorbed vertically on the TiO_2 surface, connecting linearly to the Ti_{5c} atom through the

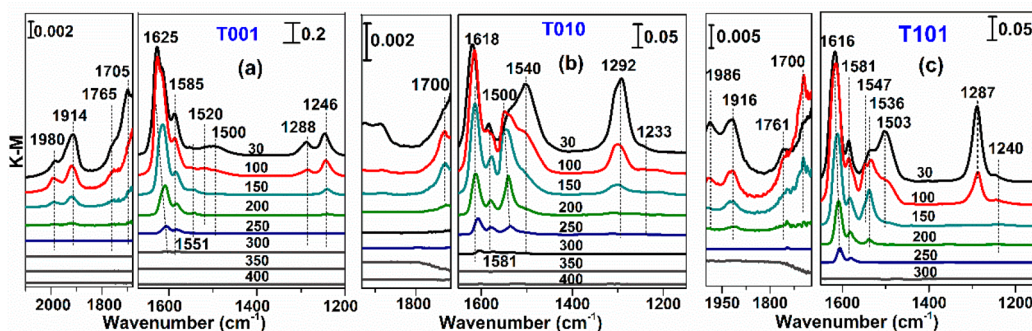


Figure 2. (a)–(c) *In situ* DRIFTS spectra of the three facets exposed to 500 ppmv NO + 5 vol % O_2 as a function of temperature. Reaction conditions: 500 ppmv NO and 5 vol % O_2 balanced with N_2 in a total flow of 300 mL/min under dry conditions.

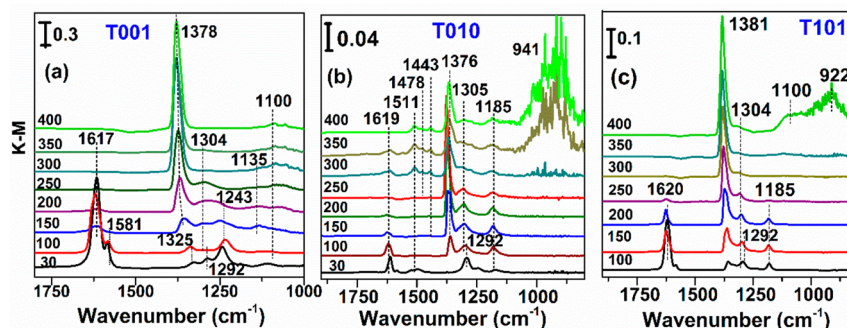


Figure 3. *In situ* DRIFTS spectra of the $\text{SO}_2 + \text{NO} + \text{O}_2$ reaction on (a) T001, (b) T010, and (c) T101 as a function of temperature. Reaction conditions: 500 ppmv NO , 50 ppmv SO_2 , and 5 vol % O_2 balanced with N_2 in a total flow of 300 mL/min under dry conditions.

N atom (Figure S2b). In the high region of 3800–3600 cm^{-1} (shown in Figure S3), the obvious consumption of OH groups indicates that they act as active sites for the adsorption and reaction of NO .³⁵

The engineered TiO_2 particles prepared in this study are in fact oxygen-deficient due to their high surface energies and low coordination structures, which is evidenced by the direct adsorption of NO on exposed Ti atoms (1986–1914, 1705–1700 cm^{-1}). Accordingly, active oxygen species can be generated through the activation of oxygen in vacancies, as confirmed by the presence of peroxy (O_2^{2-} , TiOOH) at the bands of 867, 808, and 887 cm^{-1} on T001, T010, and T101, respectively (Figure S3).^{35,51} This peroxy species may involve the oxidation of NO , thus giving rise to the formation of nitrite, NO_2 (N_2O_4), and nitrate species.

On the three facets, all the adsorption bands exhibit a decaying trend with increasing temperature. Those nitrates bear low thermal stability since corresponding bands almost vanish at 300 °C. Note that the adsorbed NO_2 dimer (N_2O_4 , 1765 cm^{-1}) emerging at low temperatures possibly remains as gaseous NO_2 at high temperatures. The gas products have been analyzed and will be discussed later.

Effect of NO on Sulfate Formation. The influence of NO on the reaction of SO_2 is investigated as a function of temperature, as shown in Figure 3. Compared to the individual reaction of SO_2 (Figure 1), larger amounts of sulfate species (approximately 1378, 1135, 1100 cm^{-1}) form with the coexistence of NO . Meanwhile, the initially formed nitrates (approximately 1617, 1581, 1292, 1243 cm^{-1}) rapidly decompose with increasing temperature and almost disappear at 200 °C, which is much lower than that (ca. 300 °C) without SO_2 (Figure 2). Concomitantly, surface nitrite (ca. 1325, 1304 cm^{-1}) is produced in this process.²⁷ It is worth mentioning that a small amount of nitrate (1619 cm^{-1}) reappears, accompanied by partial decomposition of sulfate (1376 cm^{-1}) other than production of nitrate (1511 cm^{-1}) and nitro/nitrite species (1478, 1443, 1185 cm^{-1}) above 250 °C on T010 (Figure 3b).^{52,53} The integrated areas of sulfate and nitrate formed on the three facets under different conditions also confirm this (Figure S4). There appears a significant formation of sulfate with the quick depletion of nitrate in the simultaneous reactions as opposed to the individual reactions. This means that there exists a competing effect between SO_4^{2-} and NO_3^- on TiO_2 .

DFT calculations further find that the optimized model of preadsorbed SO_4^{2-} with NO_3^- is unstable relative to that of preadsorbed NO_3^- with SO_4^{2-} , indicating that the formed sulfate would inhibit the formation of nitrate on the surface

(see details in the Supporting Information, Figure S5). In the case of T010, almost no adsorption energy difference lies in the optimized models of preadsorbed SO_4^{2-} with NO_3^- and preadsorbed NO_3^- with SO_2 . Namely, the energy barrier for the decomposition of SO_4^{2-} into SO_2 is easy to reach on T010. This may explain the abnormal decomposition of sulfate and production of nitrate and nitrite species above 250 °C on this facet.

To clarify the interaction mechanism between SO_2 and NO on the TiO_2 , the time evolution involving the reaction of preadsorbed surface species with NO or SO_2 is studied at 30 or 180 °C, as depicted in Figure 4 and Figure S6, respectively. At ambient temperature (Figure 4a), on T001, the predominant sulfite (1046 cm^{-1}) completely converts into sulfate (1105 cm^{-1}) with the following introduction of NO , while accompanying a remarkable development of nitrate species (ca. 1608, 1584, 1283, 1245 cm^{-1}). While in the other order, the introduction of SO_2 onto the nitrate-adsorbed surface gives rise to an increasing formation of sulfite (ca. 1046 cm^{-1}) but far less sulfate (1105 cm^{-1}) during a much longer duration time. The appearance of sulfate can be largely related to the enhanced adsorption of water (3460, 1650 cm^{-1}), and all these processes witness the presence of peroxide species (858 cm^{-1}).

In Figure 4b, the sulfate formation (1171 cm^{-1}) on T010 basically follows the same discipline as that found on T001, apart from other arisen nitrate/nitrite species (1530, 1500 cm^{-1} /1190 cm^{-1}) on the surface. Notably on T101 (Figure 4c), it differs from the other two facets in that sulfate (1108, 1091 cm^{-1}) is visible in the individual reaction of SO_2 , which increases and transforms into an accumulated state (1372, 1275, and 1220 cm^{-1}) by the subsequent adsorption of NO .⁵⁴ The other discrepancy is rising formation of sulfate on the nitrate-occupied (1588, 1478 cm^{-1}) surface as the predominant sulfur-containing species. The observation of condensed water (3469, 1655, 1640 cm^{-1}) and HNO_3 (1400 cm^{-1}) signifies their deep link to each other and also to the increase and accumulation of sulfate on T101.⁵⁵ Note that the band of nitrate species at ca. 1608 cm^{-1} on T101 can be overlapped by the bands of condensed water, but no bands corresponding to the condensed water are found on T010. By comparison, OH generation (3672 cm^{-1}) is observed on T001, while OH consumption (3670, 3720 cm^{-1}) occurs on T010 and T101. All these results indicate that H_2O prefers to dissociate into OH (3672 cm^{-1}) on T001, whereas it tends to adsorb molecularly on T101. This may account for the different capacities of the three facets for the sulfate formation, which will be discussed later.

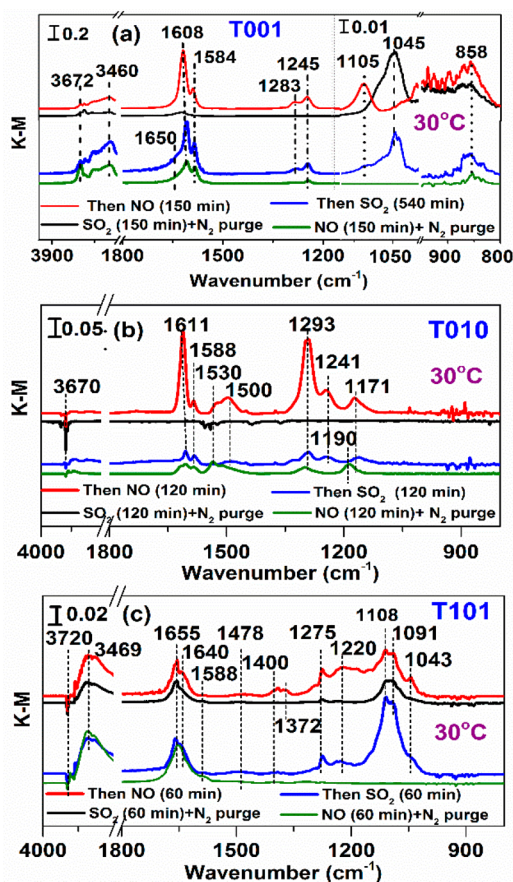


Figure 4. Comparison of the DRIFTS spectra of the individual reaction of SO_2 with that following the introduction of NO after purging with high-purity N_2 or the reverse order over (a) T001, (b) T010, and (c) T101 at 30°C . The time in brackets represents the reaction time. Reaction conditions: 5 ppmv SO_2 /10 ppmv NO and 5 vol % O_2 balanced with N_2 in a total flow of 300 mL/min under dry conditions.

Almost no difference is found with the three samples in terms of 180°C (see details in the [Supporting Information](#), Figure S6). Basically, the reaction of NO with the SO_2 -adsorbed surface gives significant sulfate accumulation (1361 cm^{-1}) at the expense of depletion of nitrate (Figure S6d-f), contrary to the other situation (Figure S6a-c). Combining with the above analysis, the NO-promoted sulfate formation appears to be related to the interaction between adsorbed sulfite with adsorbed-NO products on the surface.

Quantitative Analysis. The IC measurements are carried out to quantitatively investigate the surface products formed in the DRIFTS reactions at both 30 and 180°C (Figure 5). On all the facets, NO coexistence results in more significant formation of sulfate but less nitrate as compared to the individual reaction. A small amount of nitrite species is also detected on T001 and T010 in the simultaneous reactions at 30°C . Very little nitrate species remains despite significantly NO-promoted sulfate formation in the simultaneous reactions on all the samples at 180°C . Actually, the obtained nitrate/nitrite species can be underestimated due to their low thermal stability or easy evaporation at high temperatures, as demonstrated in the DRIFTS spectra (Figure 2). Among the three facets, NO coexistence results in the largest sulfate increment on T101 when normalized to a specific surface area, regardless of being at 30°C or at 180°C . For instance, the

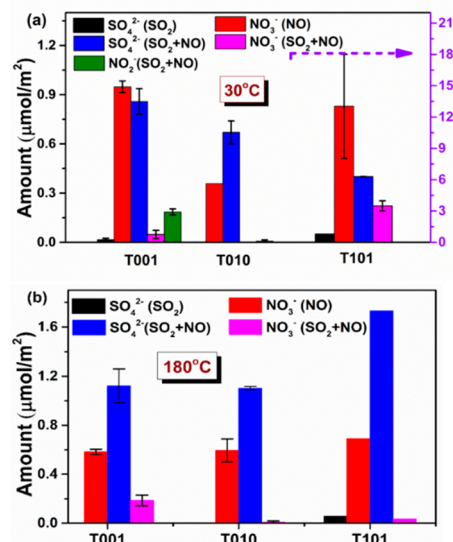


Figure 5. IC results of surface products formed on T001, T010, and T101 at (a) 30°C and (b) 180°C after the surfaces were saturated NO and/or SO_2 under dry conditions. The error bars represent the standard deviation from three independent experiments.

incremental sulfate amount reached $5.49\ \mu\text{mol m}^{-2}$ on T101 relative to $0.84\ \mu\text{mol m}^{-2}$ and $0.67\ \mu\text{mol m}^{-2}$ on T001 and T010, respectively, at ambient temperature, whereas this discrepancy narrows at 180°C on T101 mainly owing to the decreased sulfate formation.

Then we take the T001 as a representative to analyze the gas products in the heating process (see more details in the [Supporting Information](#), Figure S7). The T001 has been presaturated with reactants followed by purging with high-purity N_2 in the DRIFTS cell. As shown in Figure S7a,b, the released NO_2 from 175 to 400°C acts as oxidants for the buildup of sulfate, just as confirmed by its drastic drop with the simultaneously presorption of SO_2 . The accumulated sulfate would occupy the active sites belonging to nitrate species, thus leading to a more rapid depletion of nitrate at high temperatures, as observed by DRIFTS spectra and supported by DFT calculations (Figures 3, S4, S5). A noteworthy fact is that the released NO_2 and NO/HONO at high temperatures are from the decomposition of surface-adsorbed nitrate and nitrite (formed at low temperatures), respectively, whereas those at ambient temperature are from the oxidized NO or physically adsorbed NO, just as shown in Figure S7c.²³

The flow tube reactor is further used to investigate the kinetic uptake of SO_2 on TiO_2 (Figures S8, S9). The amounts of surface products formed on T001 and T010 are at a similar level but are much smaller than those of T101 at ambient temperature (Figure 5). Thus, we choose T001 as the subject to obtain the uptake coefficient (γ) of SO_2 , which can be integrated as a lower limit of γ on TiO_2 nanoparticles. SO_2 uptake on the quartz tube can be negligible in the blank experiments (Figure S8a). In all cases, a linear relationship between the geometric uptake coefficient (γ_{geo}) and the mass is obtained based on a series of initial uptake curves of SO_2 in the range of 0 – 8 mg (Figure S9a). The γ_t is thus calculated via eq S2 within the mass-dependence range of γ_{geo} . Figure 6 shows typical uptake curves of SO_2 over T001 in the absence and presence of NO. The coexistence of NO led to an enhanced uptake of SO_2 , with a weak increase of the γ_t from $(1.39 \pm$

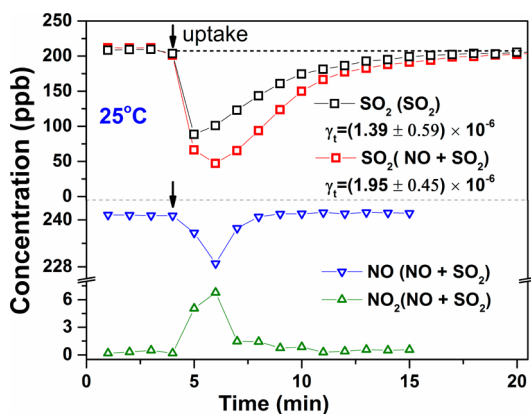


Figure 6. SO₂ uptake and NO₂ formation on T001 in the absence (3.16 mg, black) and presence (3.22 mg, red) of NO in the flow tube experiments at 0% RH. The γ_t of SO₂ in both cases was listed below the uptake curves. The solid line is drawn to guide the eye.

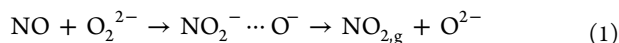
$0.59) \times 10^{-6}$ to $(1.95 \pm 0.45) \times 10^{-6}$. The yield of NO₂ observed with the simultaneous drop of NO indicates that the weakly enhanced uptake of SO₂ can be due to the generation of NO₂. Besides, a little HONO is also detected (Figure S8b).

The effect of RH on the uptake of SO₂ with the coexistence of NO is studied. As shown in Figure S9b, a negative RH dependence is found below 32% RH. The γ_t decreases from $(1.95 \pm 0.45) \times 10^{-6}$ at 0% RH to $(2.62 \pm 0.53) \times 10^{-7}$ at 32% RH, but it then increases to $(1.08 \pm 0.11) \times 10^{-6}$ with the further increase of RH to 80%. Corresponding values of the γ_t are summarized in Table S1.

Discussion of the Reaction Mechanism. Results from DRIFTS spectra reveal that the OH groups and active oxygen species (O⁻, O₂²⁻) available on all facets play fundamental roles in the heterogeneous reactions of SO₂ and/or NO. The undercoordinated structures of TiO₂ prepared in this study favor the dissociation of H₂O into OH as well as the activation of oxygen in vacancies, as commonly recognized in the literature.^{51,56–58}

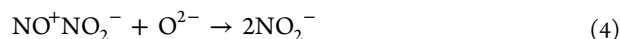
The SO₂ reaction mechanisms in this study should also be the same as previously proposed.^{9,58,59} The OH groups and lattice oxygen (O²⁻) sites interact with SO₂ to form adsorbed sulfite, whereas the O²⁻ appears to play a lesser role relative to OH because the sulfite amount should not decrease if more O²⁻ were generated due to the removal of OH in the heating process, based upon the observation on T001 (Figure 1). It is reported that the OH groups and active oxygen (O⁻) also favor the formation of sulfate, as found on T001 and T101.

With respect to the NO reaction, there is great evidence suggesting that the peroxide and NO₂ (or N₂O₄) are important intermediates for the conversion of NO into nitrate species (Figure 2). The active peroxide species (O₂²⁻) first induces NO to form a nitrite species (1185 cm⁻¹, Figure S3), which is then rapidly released as gaseous NO₂.^{43,60} As suggested from the DFT calculations, the nitrate species preferentially exists relative to gaseous NO₂ due to its lower adsorption energy. Therefore, the formed NO₂, which adsorbs on OH sites, partially transforms into stable nitrate products via a disproportionation reaction.⁵⁰ The reactions are expressed as follows.



where the formed nitrite species can be further converted to nitrate by excess NO₂.⁶¹ Those nitrate and nitrite species formed at low temperatures would decompose into gaseous NO₂ and NO or HONO at high temperatures.

The yielded NO₂ via eq 1 oxidizes the adsorbed sulfite into sulfate, while it is reduced into nitrite species via a redox process, as reported by Liu et al. and Ma et al.^{24,27}



The resulting nitrite species may remain in the reduced state with low concentration of NO₂ but excess SO₂ or partially transform into gaseous HONO once encountering H₂O molecules. These are observed in the DRIFTS spectra (1304 cm⁻¹, Figure 3) and supported by IC (Figure 5) and flow tube reactor experiments (Figure 6).^{27,62}

IC results reveal that the NO-promoted sulfate formation is most favorable on T101. A previous study found that the (101) facet has strong covalent interactions with adsorbate relative to the (001) facet.⁶³ DFT calculations from this study also indicate that the (101) facet prefers to accommodate SO₃²⁻ and NO₂, and both are key intermediates for the sulfate formation (eq 3). On the other hand, DRIFTS spectra evidence that the H₂O tends to dissociate into OH on the (001) facet while adsorbing molecularly on the (101) facet,^{64,65} whereas no adsorbed water is found on T010 (Figure 4b). At ambient temperature, the condensed water (1655, 1640 cm⁻¹, Figure 4c) residing on the top layer of the (101) facet may create an acidic microenvironment via the hydrolysis and dissociation of SO₂, which allows soluble nitrate to oxidize adsorbed sulfite, as shown below.^{30,66}



In the condensed water, the dissociative hydrogen ion may also undergo interaction with loosely bounded nitrate to form “HNO₃-like” species, as indicated by the presence of the band at 1400 cm⁻¹ on T101 (Figure 4c). In contrast, the reactions via eqs 5 and 6 can be weak on the (001) facet because only a small amount of sulfate forms with extremely low condensed water (1650 cm⁻¹) detected after a very long exposure time at 0% RH (Figure 4a). Based on all these reasons, a more significant NO-promoted sulfate formation on T101 than on T001 and T010 is reasonable. When the reaction occurs at 180 °C, the adsorbed water would leave the surface, exerting none of those roles mentioned above. This may explain the small sulfate amount formed at 180 °C as compared to that at ambient temperature on T101.

However, the role of adsorbed water is complex at elevated RH on T001 (Figure S9). The γ_t of SO₂ does not increase but decreases at 32% RH, regardless of the presence of NO. It has been reported that the γ_t of water, i.e., $(4.4 \pm 0.7) \times 10^{-2}$, is much larger than the γ_t of SO₂ obtained here.⁶⁷ This means that the water has a priority over SO₂ to adsorb on the surface. A coverage of one monolayer of water adsorbed on TiO₂ is found at approximately 11–26% RH, while that of two to four adsorbed layers is at 50–80% RH.^{68,69} In terms of this, the 32% RH allows adsorbed water to spread out over the whole surface, thus covering the active sites (i.e., OH and active oxygen species) and suppressing the formation of NO₂ and adsorbed sulfite species. Whereas with the further increase of

RH beyond 32%, multilayers of adsorbed water would contribute to the uptake of SO₂ due to the hydration of SO₂ via eq 5, hence partially counteracting its negative effect.³⁰ Therefore, the γ_t increases again from 32% to 80% RH.

Implications for Local Atmospheric Environment. As suggested from the results of DRIFTS spectra, flow tube reactor experiments, and IC measurements, we propose a new potential pathway for the formation of sulfate in the areas of power plants containing high concentrations of NO, SO₂, and high-defect TiO₂ nanoparticles. The coexistence of NO could contribute greatly to the formation of sulfate species on the TiO₂-relevant catalysts. As the emitted TiO₂ particles from attributed TiO₂-containing catalysts undergo transport inside the stack, they may encounter NO and SO₂ in plumes. The high-temperature flue gas favors the oxidation of SO₂ in the presence of NO, leading to unanticipated emission of sulfate species. Besides, the formed sulfate may also stick inside the stack, causing plug problems and additional burden on the tube cleaning.

As indicated by the DRIFTS spectra, the active oxygen species stemming from the activation of oxygen in the vacancies play a fundamental role in the dark conversion of NO to NO₂ on TiO₂ nanoparticles. Evidence from gas product analysis and flow tube reactor experiments confirm the yield of NO₂. Further formation of sulfate involving a redox reaction between NO₂ and SO₂ occurs, along with the generation of nitrite and HONO byproducts (which possibly act as a potential source of HONO and OH radicals).⁷⁰ The facile availability of oxide powders with vacancies in the atmosphere as well as similar reports on other oxides at high temperatures (albeit with different mechanism proposed) reminds us of its possibility of occurring on common mineral dusts in the atmosphere.^{22,23,58} A previous study reported that the high reactivity of TiO₂ dust toward the oxidation of SO₂ is generally associated with a light-driven photochemical process, in which TiO₂ acts as a photocatalyst initiating the formation of gaseous OH radicals,⁴ whereas our results imply that the sulfate formation may also occur without light radiance but with the aid of active oxygen species-initiated NO₂ formation over nighttime.

Although the obtained γ_t of SO₂ with the coexistence of NO on the (001) facet was lower than recommended for an appreciable impact on heterogeneous reactions, it can be taken as a lower limit, and the contribution of NO to the sulfate formation can be underestimated considering the much larger promotion effect found on the (101) facet.⁷¹ Actually, the (101) facet is the most available facet (dominating a greater than 94% fraction) in ubiquitous anatase TiO₂ dust, irrespective of being from natural or anthropogenic sources.^{30,72,73} Based on the possible occurrence of the promotion effect on other oxides as above-mentioned, a more comprehensive kinetics study on other typical dusts should be carried out to fully evaluate the role of NO in the heterogeneous reaction of SO₂.

Lastly, the finding in this study hints that the (001) and (010) facets could be a better option for the design of widely applied TiO₂-based catalysts, combined with their superior activity (which has been commonly recognized) as well as a lesser role in the NO-promoted sulfate formation. This would be beneficial for air pollution remediation.

■ ASSOCIATED CONTENT

Supporting Information

The Supporting Information is available free of charge on the ACS Publications website at DOI: 10.1021/acs.est.8b02688.

XRD and TEM patterns of the three TiO₂ samples; DFT calculations for optimized adsorption structures and adsorption energies of reactants and products on different facets; DRIFTS spectra of NO reaction versus time on the three facets; comparison of the integrated areas for nitrate and sulfate formed on the three facets with temperature; DRIFTS spectra of SO₂ reaction with preadsorbed NO species and the reverse order at 180 °C; mass-dependent γ_{geo} of SO₂ with and without NO at different RH on T001; gas product analysis (PDF)

■ AUTHOR INFORMATION

Corresponding Author

*Phone: 86-17786507005. E-mail: guoyanbing@mail.ccnu.edu.cn.

ORCID

Weiwei Yang: 0000-0002-9227-0459

Yanbing Guo: 0000-0002-5399-1739

Lizhi Zhang: 0000-0002-6842-9167

Notes

The authors declare no competing financial interest.

■ ACKNOWLEDGMENTS

The work is financially supported by the Recruitment Program of Global Young Experts start-up funds and the Program of Introducing Talents of Discipline to Universities of China (111 program, B17019), the National Natural Science Foundation of China (nos. 21707039, 21777051), the Project funded by the China Postdoctoral Science Foundation (no. 2017M622485), and National Engineering Laboratory for Mobile Source Emission Control Technology (NELM-S2017A11).

■ REFERENCES

- (1) Zhang, R.; Wang, G.; Guo, S.; Zamora, M. L.; Ying, Q.; Lin, Y.; Wang, W.; Hu, M.; Wang, Y. Formation of urban fine particulate matter. *Chem. Rev.* **2015**, *115* (10), 3803–3855.
- (2) Wang, G.; Zhang, R.; Gomez, M. E.; Yang, L.; Levy Zamora, M.; Hu, M.; Lin, Y.; Peng, J.; Guo, S.; Meng, J.; Li, J.; Cheng, C.; Hu, T.; Ren, Y.; Wang, Y.; Gao, J.; Cao, J.; An, Z.; Zhou, W.; Li, G.; Wang, J.; Tian, P.; Marrero-Ortiz, W.; Secret, J.; Du, Z.; Zheng, J.; Shang, D.; Zeng, L.; Shao, M.; Wang, W.; Huang, Y.; Wang, Y.; Zhu, Y.; Li, Y.; Hu, J.; Pan, B.; Cai, L.; Cheng, Y.; Ji, Y.; Zhang, F.; Rosenfeld, D.; Liss, P. S.; Duce, R. A.; Kolb, C. E.; Molina, M. J. Persistent sulfate formation from London Fog to Chinese haze. *Proc. Natl. Acad. Sci. U. S. A.* **2016**, *113*, 13630–13635.
- (3) Guo, S.; Hu, M.; Zamora, M. L.; Peng, J.; Shang, D.; Zheng, J.; Du, Z.; Wu, Z.; Shao, M.; Zeng, L.; Molina, M. J.; Zhang, R. Elucidating severe urban haze formation in China. *Proc. Natl. Acad. Sci. U. S. A.* **2014**, *111* (49), 17373–17378.
- (4) Dupart, Y.; King, S. M.; Nekat, B.; Nowak, A.; Wiedensohler, A.; Herrmann, H.; Gregory, D.; Thomas, B.; Miffre, A.; Rairoux, P.; D'Anna, B.; George, C. Mineral dust photochemistry induces nucleation events in the presence of SO₂. *Proc. Natl. Acad. Sci. U. S. A.* **2012**, *109* (51), 20842–20847.
- (5) Li, G.; Bei, N.; Cao, J.; Huang, R.; Wu, J.; Feng, T.; Wang, Y.; Liu, S.; Zhang, Q.; Tie, X.; Molina, L. T. A possible pathway for rapid growth of sulfate during haze days in China. *Atmos. Chem. Phys.* **2017**, *17*, 3301–3316.

- (6) Nicolas, M.; Ndour, M.; Ka, O.; D'Anna, B.; George, C. Photochemistry of Atmospheric Dust: Ozone Decomposition on Illuminated Titanium Dioxide. *Environ. Sci. Technol.* **2009**, *43*, 7437–7442.
- (7) Tang, M. J.; Telford, P. J.; Pope, F. D.; Rkhouak, L.; Abraham, N. L.; Archibald, A. T.; Braesicke, P.; Pyle, J. A.; McGregor, J.; Watson, I. M.; Cox, R. A.; Kalberer, M. Heterogeneous reaction of N_2O_5 with airborne TiO_2 particles and its implication for stratospheric particle injection. *Atmos. Chem. Phys.* **2014**, *14* (12), 6035–6048.
- (8) Grassian, V. H. New Directions: Nanodust – A source of metals in the atmospheric environment. *Atmos. Environ.* **2009**, *43*, 6119.
- (9) Baltrusaitis, J.; Jayaweera, P. M.; Grassian, V. H. Sulfur Dioxide Adsorption on TiO_2 Nanoparticles: Influence of Particle Size, Coadsorbates, Sample Pretreatment, and Light on Surface Speciation and Surface Coverage. *J. Phys. Chem. C* **2011**, *115*, 492–500.
- (10) Nanayakkara, C. E.; Pettibone, J.; Grassian, V. H. Sulfur dioxide adsorption and photooxidation on isotopically-labeled titanium dioxide nanoparticle surfaces: roles of surface hydroxyl groups and adsorbed water in the formation and stability of adsorbed sulfite and sulfate. *Phys. Chem. Chem. Phys.* **2012**, *14* (19), 6957–6966.
- (11) Usher, C. R.; Michel, A. E.; Grassian, V. H. Reactions on Mineral Dust. *Chem. Rev.* **2003**, *103*, 4883–4939.
- (12) Tang, M.; Cziczko, D. J.; Grassian, V. H. Interactions of Water with Mineral Dust Aerosol: Water Adsorption, Hygroscopicity, Cloud Condensation, and Ice Nucleation. *Chem. Rev.* **2016**, *116* (7), 4205–4259.
- (13) Linsebigler, A. L.; Lu, G. Q.; Yates, J. J. T. Photocatalysis on TiO_2 Surfaces: Principles, Mechanisms, and Selected Results. *Chem. Rev.* **1995**, *95*, 735–758.
- (14) Warburton, D. R.; Purdie, D.; Murny, C. A.; Prabhakaran, K.; Wincott, P. L.; Thornton, G. NEXAFS fingerprinting of $\text{TiO}_2(110)\text{-SO}_2$. *Surf. Sci.* **1992**, *269-270*, 305–309.
- (15) Smith, K.; Mackay, J.; Henrich, V. Interaction of SO_2 with nearly perfect and defect $\text{TiO}_2(110)$ surfaces. *Phys. Rev. B: Condens. Matter Mater. Phys.* **1987**, *35* (11), S822–S829.
- (16) Srivastava, R. K.; Miller, C. A.; Erickson, C.; Jambhekar, R. Emission of Sulfur Trioxide from Coal Fired Power Plants. *J. Air Waste Manage. Assoc.* **2004**, *54*, 750–762.
- (17) Saikawa, E.; Kim, H.; Zhong, M.; Avramov, A.; Zhao, Y.; Janssens-Maenhout, G.; Kurokawa, J.; Klimont, Z.; Wagner, E.; Naik, V.; Horowitz, L. W.; Zhang, Q. Comparison of emissions inventories of anthropogenic air pollutants and greenhouse gases in China. *Atmos. Chem. Phys.* **2017**, *17*, 6393–6421.
- (18) Junkermann, W.; Vogel, B.; Sutton, M. A. The climate penalty for clean fossil fuel combustion. *Atmos. Chem. Phys.* **2011**, *11* (24), 12917–12924.
- (19) Lonsdale, C. R.; Stevens, R. G.; Brock, C. A.; Makar, P. A.; Knipping, E. M.; Pierce, J. R. The effect of coal-fired power-plant SO_2 and NO_x control technologies on aerosol nucleation in the source plumes. *Atmos. Chem. Phys.* **2012**, *12* (23), 11519–11531.
- (20) Wei, Z.; Li, X.; Xu, L.; Cheng, Y. Comparative study of computational intelligence approaches for NO_x reduction of coal-fired boiler. *Energy* **2013**, *55*, 683–692.
- (21) Walters, W. W.; Tharp, B. D.; Fang, H.; Kozak, B. J.; Michalski, G. Nitrogen Isotope Composition of Thermally Produced NO_x from Various Fossil-Fuel Combustion Sources. *Environ. Sci. Technol.* **2015**, *49* (19), 11363–11371.
- (22) Ishizuka, T.; Hajime, K.; Tsutomu, Y. Initial step of flue gas desulfurization-an IR study of the reaction of SO_2 with NO_x on CaO . *Environ. Sci. Technol.* **2000**, *34*, 2799–2803.
- (23) Xie, Y.; Chen, Y.; Ma, Y.; Jin, Z. Investigation of simultaneous adsorption of SO_2 and NO on gamma-alumina at low temperature using DRIFTS. *J. Hazard. Mater.* **2011**, *195*, 223–229.
- (24) Liu, C.; Ma, Q.; Liu, Y.; Ma, J.; He, H. Synergistic reaction between SO_2 and NO_2 on mineral oxides: a potential formation pathway of sulfate aerosol. *Phys. Chem. Chem. Phys.* **2012**, *14*, 1668–1676.
- (25) He, H.; Wang, Y.; Ma, Q.; Ma, J.; Chu, B.; Ji, D.; Tang, G.; Liu, C.; Zhang, H.; Hao, J. Mineral dust and NO_x promote the conversion of SO_2 to sulfate in heavy pollution days. *Sci. Rep.* **2015**, *4*, 4172–4176.
- (26) Han, C.; Yang, W.; Wu, Q.; Yang, H.; Xue, X. Heterogeneous Photochemical Conversion of NO_2 to HONO on the Humic Acid Surface under Simulated Sunlight. *Environ. Sci. Technol.* **2016**, *50* (10), 5017–5023.
- (27) Ma, Q.; Wang, T.; Liu, C.; He, H.; Wang, Z.; Wang, W.; Liang, Y. SO_2 Initiates the Efficient Conversion of NO_2 to HONO on MgO Surface. *Environ. Sci. Technol.* **2017**, *51*, 3767–3775.
- (28) Ndour, M.; D'Anna, B.; George, C.; Ka, O.; Balkanski, Y.; Kleffmann, J.; Stemmler, K.; Ammann, M. Photoenhanced uptake of NO_2 on mineral dust: Laboratory experiments and model simulations. *Geophys. Res. Lett.* **2008**, DOI: 10.1029/2007GL032006.
- (29) Liu, Y.; Han, C.; Ma, J.; Bao, X.; He, H. Influence of relative humidity on heterogeneous kinetics of NO_2 on kaolin and hematite. *Phys. Chem. Chem. Phys.* **2015**, *17* (29), 19424–19431.
- (30) Huang, L.; Zhao, Y.; Li, H.; Chen, Z. Kinetics of Heterogeneous Reaction of Sulfur Dioxide on Authentic Mineral Dust: Effects of Relative Humidity and Hydrogen Peroxide. *Environ. Sci. Technol.* **2015**, *49* (18), 10797–805.
- (31) Yang, W.; He, H.; Ma, Q.; Ma, J.; Liu, Y.; Liu, P.; Mu, Y. Synergistic formation of sulfate and ammonium resulting from reaction between SO_2 and NH_3 on typical mineral dust. *Phys. Chem. Chem. Phys.* **2016**, *18*, 956–964.
- (32) Saur, O.; Bensitel, M.; Mohammed Saad, A. B.; Lavalley, J. C.; Tripp, C. P.; Morrow, B. A. The Structure and Stability of Sulfated Alumina and Titania. *J. Catal.* **1986**, *99*, 104–110.
- (33) Nakajima, F.; Hamada, I. The state-of-the-art technology of NO_x control. *Catal. Today* **1996**, *29*, 109–115.
- (34) Deiana, C.; Fois, E.; Coluccia, S.; Martra, G. Surface Structure of TiO_2 P25 Nanoparticles Infrared Study of Hydroxy Groups on Coordinative Defect Sites. *J. Phys. Chem. C* **2010**, *114*, 21531–21538.
- (35) Wu, J.; Cheng, Y. In situ FTIR study of photocatalytic NO reaction on photocatalysts under UV irradiation. *J. Catal.* **2006**, *237*, 393–404.
- (36) Primet, M.; Pichat, P.; Mathieu, M. V. Infrared Study of the Surface of Titanium Dioxides. I. Hydroxyl groups. *J. Phys. Chem.* **1971**, *75*, 1216–1220.
- (37) Liu, F.; Asakura, K.; He, H.; Shan, W.; Shi, X.; Zhang, C. Influence of sulfation on iron titanate catalyst for the selective catalytic reduction of NO_x with NH_3 . *Appl. Catal., B* **2011**, *103* (3–4), 369–377.
- (38) Wu, H.; Cai, W.; Long, M.; Wang, H.; Wang, Z.; Chen, C.; Hu, X.; Yu, X. Sulfur Dioxide Capture by Heterogeneous Oxidation on Hydroxylated Manganese Dioxide. *Environ. Sci. Technol.* **2016**, *50* (11), 5809–5916.
- (39) Pan, X.; Yang, M. Q.; Fu, X.; Zhang, N.; Xu, Y. J. Defective TiO_2 with oxygen vacancies: synthesis, properties and photocatalytic applications. *Nanoscale* **2013**, *5* (9), 3601–3614.
- (40) Zhang, X.; Zhuang, G.; Chen, J.; Wang, Y.; Wang, X.; An, Z.; Zhang, P. Heterogeneous reactions of sulfur dioxide on typical mineral particles. *J. Phys. Chem. B* **2006**, *110*, 12588–12596.
- (41) Jiang, B. Q.; Wu, Z. B.; Liu, Y.; Lee, S. C.; Ho, W. K. DRIFT Study of the SO_2 Effect on Low-Temperature SCR Reaction over Fe-Mn/ TiO_2 . *J. Phys. Chem. C* **2010**, *114* (11), 4961–4965.
- (42) Piazzesi, G.; Elsener, M.; Kröcher, O.; Wokaun, A. Influence of NO_2 on the hydrolysis of isocyanic acid over TiO_2 . *Appl. Catal., B* **2006**, *65*, 169–174.
- (43) Huang, L.; Zha, K.; Namuangruk, S.; Junkaew, A.; Zhao, X.; Li, H.; Shi, L.; Zhang, D. Promotional effect of the $\text{TiO}_2(001)$ facet in the selective catalytic reduction of NO with NH_3 : in situ DRIFTS and DFT studies. *Catal. Sci. Technol.* **2016**, *6* (24), 8516–8524.
- (44) Wang, W.; McCool, G.; Kapur, N.; Yuan, G.; Shan, B.; Nguyen, M.; Graham, U. M.; Davis, B. H.; Jacobs, G.; Cho, K.; Hao, X. K. Mixed-Phase Oxide Catalyst Based on Mn-Mullite (Sm, Gd) Mn_2O_5 for NO Oxidation in Diesel Exhaust. *Science* **2012**, *337*, 832–835.
- (45) Mikhaylov, R. V.; Lisachenko, A. A.; Shelimov, B. N.; Kazansky, V. B.; Martra, G.; Coluccia, S. FTIR and TPD Study of the Room

Temperature Interaction of a NO–Oxygen Mixture and of NO₂ with Titanium Dioxide. *J. Phys. Chem. C* **2013**, *117* (20), 10345–10352.

(46) Hixson, B. C.; Jordan, J. W.; Wagner, E. L.; Bevssek, H. M. Reaction products and kinetics of the reaction of NO₂ with gamma-Fe₂O₃. *J. Phys. Chem. A* **2011**, *115* (46), 13364–13369.

(47) Niu, H.; Li, K.; Chu, B.; Su, W.; Li, J. Heterogeneous Reactions between Toluene and NO₂ on Mineral Particles under Simulated Atmospheric Conditions. *Environ. Sci. Technol.* **2017**, *51*, 9596–9604.

(48) Lesko, D. M.; Coddens, E. M.; Swomley, H. D.; Welch, R. M.; Borgatta, J.; Navea, J. G. Photochemistry of nitrate chemisorbed on various metal oxide surfaces. *Phys. Chem. Chem. Phys.* **2015**, *17* (32), 20775–20785.

(49) Tan, F.; Tong, S.; Jing, B.; Hou, S.; Liu, Q.; Li, K.; Zhang, Y.; Ge, M. Heterogeneous reactions of NO₂ with CaCO₃–(NH₄)₂SO₄ mixtures at different relative humidities. *Atmos. Chem. Phys.* **2016**, *16*, 8081–8093.

(50) Borensen, C.; Kirchner, U.; Scheer, V.; Vogt, R.; Zellner, R. Mechanism and Kinetics of the Reactions of NO₂ or HNO₃ with Alumina as a Mineral Dust Model Compound. *J. Phys. Chem. A* **2000**, *104*, 5036–5045.

(51) Setvin, M.; Aschauer, U.; Scheiber, P.; Li, Y. F.; Hou, W.; Schmid, M.; Selloni, A.; Diebold, U. Reaction of O₂ with Subsurface Oxygen Vacancies on TiO₂ Anatase (101). *Science* **2013**, *341* (6149), 988–991.

(52) Hadjiivanov, K. I. Identification of Neutral and Charged N_xO_y Surface Species by IR Spectroscopy. *Catal. Rev.: Sci. Eng.* **2000**, *42* (1–2), 71–144.

(53) Mikhaylov, R. V.; Lisachenko, A. A.; Shelimov, B. N.; Kazansky, V. B.; Martra, G.; Coluccia, S. FTIR and TPD Study of the Room Temperature Interaction of a NO–Oxygen Mixture and of NO₂ with Titanium Dioxide. *J. Phys. Chem. C* **2013**, *117*, 10345–10352.

(54) Wu, Q.; Gao, H.; He, H. Conformational Analysis of Sulfate Species on Ag–Al₂O₃ by Means of Theoretical and Experimental Vibration Spectra. *J. Phys. Chem. B* **2006**, *110*, 8320–8324.

(55) Rubasinghege, G.; Grassian, V. H. Role(s) of adsorbed water in the surface chemistry of environmental interfaces. *Chem. Commun.* **2013**, *49* (30), 3071–3094.

(56) Schaub, R.; Thostrup, P.; Lopez, N.; Laegsgaard, E.; Stensgaard, I.; Norskov, J. K.; Besenbacher, F. Oxygen vacancies as active sites for water dissociation on rutile TiO₂ (110). *Phys. Rev. Lett.* **2001**, *87* (26), 266104.

(57) Deiana, C.; Fois, E.; Coluccia, S.; Martra, G. Surface Structure of TiO₂ P25 Nanoparticles: Infrared Study of Hydroxy Groups on Coordinative Defect Sites. *J. Phys. Chem. C* **2010**, *114*, 21531–21538.

(58) Baltrusaitis, J.; Cwiertny, D. M.; Grassian, V. H. Adsorption of sulfur dioxide on hematite and goethite particle surfaces. *Phys. Chem. Chem. Phys.* **2007**, *9*, 5542–5554.

(59) Rodriguez, J. A.; Jirsak, T.; Freitag, A.; Larese, J. Z. Interaction of SO₂ with MgO(100) and Cu/MgO(100): Decomposition Reactions and the Formation of SO₃ and SO₄. *J. Phys. Chem. B* **2000**, *104*, 7439–7448.

(60) Gao, F.; Tang, X.; Yi, H.; Chu, C.; Li, N.; Li, J.; Zhao, S. In-situ DRIFTS for the mechanistic studies of NO oxidation over α -MnO₂, β -MnO₂ and γ -MnO₂ catalysts. *Chem. Eng. J.* **2017**, *322*, 525–537.

(61) Underwood, G. M.; Miller, T. M.; Grassian, V. H. Transmission FT-IR and Knudsen Cell Study of the Heterogeneous Reactivity of Gaseous Nitrogen Dioxide on Mineral Oxide Particles. *J. Phys. Chem. A* **1999**, *103*, 6184–6190.

(62) Liu, W.; He, X.; Pang, S.; Zhang, Y. Effect of relative humidity on O₃ and NO₂ oxidation of SO₂ on α -Al₂O₃ particles. *Atmos. Environ.* **2017**, *167*, 245–253.

(63) Li, C.; Koenigsman, C.; Ding, W.; Rudshteyn, B.; Yang, K. R.; Regan, K. P.; Konezny, S. J.; Batista, V. S.; Brudvig, G. W.; Schmuttenmaer, C. A.; Kim, J. H. Facet-dependent photoelectrochemical performance of TiO₂ nanostructures: an experimental and computational study. *J. Am. Chem. Soc.* **2015**, *137* (4), 1520–1529.

(64) Zhao, Z.; Li, Z.; Zou, Z. Understanding the interaction of water with anatase TiO₂ (101) surface from density functional theory calculations. *Phys. Lett. A* **2011**, *375* (32), 2939–2945.

(65) Zhao, Y.; Ma, W.; Li, Y.; Ji, H.; Chen, C.; Zhu, H.; Zhao, J. The surface-structure sensitivity of dioxygen activation in the anatase-photocatalyzed oxidation reaction. *Angew. Chem., Int. Ed.* **2012**, *51* (13), 3188–3192.

(66) Kong, L. D.; Zhao, X.; Sun, Z. Y.; Yang, Y. W.; Fu, H. B.; Zhang, S. C.; Cheng, T. T.; Yang, X.; Wang, L.; Chen, J. M. The effects of nitrate on the heterogeneous uptake of sulfur dioxide on hematite. *Atmos. Chem. Phys.* **2014**, *14* (17), 9451–9467.

(67) Seisel, S.; Lian, Y.; Keil, T.; Trukhin, M. E.; Zellner, R. Kinetics of the interaction of water vapour with mineral dust and soot surfaces at T = 298K. *Phys. Chem. Chem. Phys.* **2004**, *6* (8), 1926–1932.

(68) Ma, Q.; He, H.; Liu, Y. In situ DRIFTS study of hygroscopic behavior of mineral aerosol. *J. Environ. Sci.* **2010**, *22* (4), 555–560.

(69) Goodman, A. L.; Bernard, E. T.; Grassian, V. H. Spectroscopic Study of Nitric Acid and Water Adsorption on Oxide Particles: Enhanced Nitric Acid Uptake Kinetics in the Presence of Adsorbed Water. *J. Phys. Chem. A* **2001**, *105*, 6443–6457.

(70) Su, H.; Cheng, Y.; Oswald, R.; Behrendt, T.; Trebs, I.; Meixner, F. X.; Andreae, M. O.; Cheng, P.; Zhang, Y.; Pöschl, U. Soil Nitrite as a Source of Atmospheric HONO and OH Radicals. *Science* **2011**, *333*, 1616–1618.

(71) Crowley, J. N.; Ammann, M.; Cox, R. A.; Hynes, R. G.; Jenkin, M. E.; Mellouki, A.; Rossi, M. J.; Troe, J.; Wallington, T. J. Evaluated kinetic and photochemical data for atmospheric chemistry: Volume V – heterogeneous reactions on solid substrates. *Atmos. Chem. Phys.* **2010**, *10* (18), 9059–9223.

(72) Wang, L.; Zang, L.; Zhao, J.; Wang, C. Green synthesis of shape-defined anatase TiO₂ nanocrystals wholly exposed with {001} and {100} facets. *Chem. Commun.* **2012**, *48* (96), 11736–11738.

(73) Hou, S.; Tong, S.; Ge, M.; An, J. Comparison of atmospheric nitrous acid during severe haze and clean periods in Beijing, China. *Atmos. Environ.* **2016**, *124*, 199–206.